# Heterodyne-Detected Dispersed Vibrational Echo Spectroscopy

**Kevin C. Jones, Ziad Ganim, and Andrei Tokmakoff***

*Department of Chemistry, Massachusetts Institute of Technology, 77 Massachusetts Avenue, 6-213 Cambridge, Massachusetts 02139*

*Received: July 2, 2009; Revised Manuscript Received: November 4, 2009*

We develop heterodyned dispersed vibrational echo spectroscopy (HDVE) and demonstrate the new capabilities in biophysical applications. HDVE is a robust ultrafast technique that provides a characterization of the real and imaginary components of third-order nonlinear signals with high sensitivity and single-laser-shot capability and can be used to extract dispersed pump−probe and dispersed vibrational echo spectra. Four methods for acquiring HDVE phase and amplitude spectra were compared: Fourier transform spectral interferometry, a new phase modulation spectral interferometry technique, and combination schemes. These extraction techniques were demonstrated in the context of protein amide I spectroscopy. Experimental HDVE and heterodyned free induction decay amide I spectra were explicitly compared to conventional dispersed pump−probe, dispersed vibrational echo, and absorption spectra. The new capabilities of HDVE were demonstrated by acquiring single-shot spectra and melting curves of ubiquitin and concentration-dependent spectra of insulin suitable for extracting the binding constant for dimerization. The introduced techniques will prove particularly useful in transient experiments, studying irreversible reactions, and micromolar concentration studies of small proteins.

## I. Introduction

Due to their structural sensitivity and ultrafast time resolution, femtosecond nonlinear infrared (IR) spectroscopies are increasingly being used in studies of chemical dynamics in solution and biophysical assays of proteins,[1,2] peptides,[3] and nucleic acids[4] to reveal structure- and time-dependent changes. Third-order nonlinear vibrational spectroscopy is particularly powerful because the use of multiple pulses maps out vibrational couplings, measures anharmonicities, and can separate homogeneous and inhomogeneous contributions to absorption lineshapes. Each of these features ultimately increases structural sensitivity and aids in the ability to resolve overlapping peaks.[5] Two-dimensional infrared (2D IR) spectroscopy is the most complete characterization of the third-order vibrational response, but methods that retain nonlinear information and can be acquired and processed quickly or can be used in single-laser-shot mode are in demand for probing transient and/or irreversible chemical and biophysical dynamics. Two frequency-dispersed probing techniques, dispersed pump−probe (DPP) and dispersed vibrational echo (DVE), meet these requirements, yet they have certain disadvantages.[6] DPP spectra scale linearly with population and are related to changes in sample absorption, but signal levels are small and phase extraction requires certain assumptions. DVE spectra are background free, but, as amplitude-squared measurements, they have signal cross terms that make proportionality to concentration or structure ambiguous. Also, since DVE scales as electric field squared, its intensity scales unfavorably for samples in dilute solutions or with weak transitions.

In this work, we report on the development and characterization of methods that provide linear and phase-sensitive detection of the third-order nonlinear response. Heterodyne detection[7] has been an invaluable method for amplifying and characterizing the weak signal electric field in third-order measurements,[8] but 2D IR relies on a Fourier transform (FT) of a set of time domain data to separate phase and amplitude information. Applying a number of alternate phase-sensitive detection protocols, we developed heterodyned dispersed vibrational echo (HDVE) spectroscopy, a single-dimension frequency domain measurement of the signal generated by three time-coincident femtosecond infrared pulses. HDVE is related to the projection of the 2D IR spectrum onto the detection axis and, therefore, like DPP and DVE carries the cross-peak information of the 2D IR spectrum but may be collected ∼250−500 times faster than a 2D IR data set. In addition, the HDVE measurement can be used to reconstruct both DVE and DPP spectra. Additionally, we show that the complex linear response can be extracted from an analogous broad band heterodyne-detected measurement of the free induction decay (FID), similar to methods that have been used in the optical and terahertz regimes.[9,10] The new capabilities are demonstrated using protein amide I HDVE spectroscopy to measure the melting curve of ubiquitin and the dissociation constant of insulin and to extract the DPP and DVE spectra of ubiquitin from a single laser shot.

## II. Signal Detection Methods

**A. Heterodyne Detection.** In both linear and nonlinear ultrafast coherent spectroscopy, the signal electric field is radiated as a result of the polarization induced in the sample by incident laser pulses. This real, time-domain field, $E'(t)$, can be expressed through a FT as a complex spectral field, $\tilde{E}(\omega)$, with amplitude, $e$, and phase, $\phi$

$$\tilde{E}(\omega) = e(\omega)\exp(i\phi(\omega)) \tag{2.1}$$

Heterodyne detection of this field is accomplished by collecting an interferogram after mixing with a local oscillator field (LO), $\tilde{E}_{LO}$, separated by a time delay $\tau_{LO}$. For spectral interferometry, the measured intensity in the frequency domain $I(\omega;\tau_{LO})$ is

* To whom correspondence should be addressed. Phone: (617) 253-4503. Fax: (617) 253-7030. E-mail: tokmakof@mit.edu.

10.1021/jp906256s 
Published on Web 11/25/2009

$$I(\omega;\tau_{LO}) = |\tilde{E}_{sig}(\omega) + \tilde{E}_{LO}(\omega)\exp(-i\omega\tau_{LO})|^2 = e_{LO}^2(\omega) + e_{sig}^2(\omega) + 2e_{sig}(\omega)e_{LO}(\omega)\cos[\Delta\phi(\omega) + \tau_{LO}\omega] \quad (2.2)$$

Through phase or amplitude modulation, the spectral interferogram can be obtained by subtracting the square terms to leave the cross term

$$S'(\omega;\tau_{LO}) = 2e_{sig}(\omega)e_{LO}(\omega)\cos[\Delta\phi(\omega) + \tau_{LO}\omega] \quad (2.3)$$

The cross term amplifies the signal intensity and creates linear proportionality between the measured intensity change and electric field amplitude. The cross term is also sensitive to the phase difference between the signal and LO

$$\Delta\phi(\omega) = \phi_{sig}(\omega) - \phi_{LO}(\omega) \quad (2.4)$$

In order to extract the phase difference, the quadrature spectral interferogram component, $S''$, which may be calculated through Kramers−Kronig relations or phase modulation, is used

$$S''(\omega;\tau_{LO}) = 2e_{sig}(\omega)e_{LO}(\omega)\sin[\Delta\phi(\omega) + \tau_{LO}\omega] \quad (2.5)$$

In the text, $S'$ denotes the in-phase, real, or cosine component of the spectral interferogram while $S''$denotes the in-quadrature, imaginary, or sine component. We also define a complex spectral interferogram $\tilde{S} \equiv S' + iS''$.

***Heterodyned Ultrafast Free Induction Decay.*** The complex linear spectrum may be measured through heterodyne detection of an ultrafast broad band pulse transmitted through the sample. In this case, the transmitted electric field is

$$\tilde{E}_{sig}^{(1)}(\omega) = \tilde{E}_0(\omega)\exp[i\tilde{n}(\omega)\omega l/c] \quad (2.6)$$

where $\tilde{E}_0(\omega)$ is the beam that enters the sample, $l$ is the path length, $c$ is the speed of light, and $\tilde{n}(\omega)$ is the complex refractive index, $\tilde{n}(\omega) = n(\omega) + i\kappa(\omega)$, that has dispersive, $n(\omega)$, and absorptive, $\kappa(\omega)$, components.[9] From eq 2.3, the measured heterodyned free induction decay (HFID) can be expressed as

$$S'_{HFID}(\omega;\tau_{LO}) = 2e_0(\omega)e_{LO}(\omega)\exp[-\kappa(\omega)\omega l/c]\cos[\Delta\phi_{0,LO}(\omega) + n(\omega)\omega l/c + \tau_{LO}\omega] \quad (2.7)$$

Here, $\Delta\phi_{0,LO}$ is the phase difference between the incident excitation field and local oscillator. For comparison, the intensity of the transmitted infrared beam, which is used in conventional absorption spectroscopy, is given by

$$I_{IR}(\omega) = |\tilde{E}_0(\omega)\exp[i\tilde{n}(\omega)\omega l/c]|^2 = e_0(\omega)^2\exp[-2\kappa(\omega)\omega l/c] \quad (2.8)$$

Conventional absorption measurements only measure the change in the absorptive component of a sample relative to a reference $\Delta\kappa(\omega) = \kappa_s(\omega) - \kappa_{ref}(\omega)$, whereas the HFID can measure both $\Delta\kappa(\omega)$ and the real index change $\Delta n(\omega) = n_s(\omega) - n_{ref}(\omega)$. For either conventional absorption (eq 2.8) or HFID spectral interferogram (eq 2.7), the $\Delta\kappa(\omega)$ difference is calculated from the intensity

$$\Delta\kappa(\omega) = -\frac{\ln(10)c}{2\omega l}\log\frac{I_{IR}^{s}(\omega)}{I_{IR}^{ref}(\omega)} = -\frac{\ln(10)c}{2\omega l}\log\frac{|\tilde{S}_{HFID}^{s}(\omega;\tau_{LO})|^2}{|\tilde{S}_{HFID}^{ref}(\omega;\tau_{LO})|^2} \quad (2.9)$$

$\Delta n(\omega)$ can be extracted by subtracting the sample and reference phases from eq 2.7; the remaining $\tau_{LO}\omega$ and $\Delta\phi_{0,LO}(\omega)$ terms cancel without needing to know their absolute values.[9]

***Heterodyned Ultrafast Nonlinear Spectroscopy.*** In this work, nonlinear signal characterization is described for three third-order spectroscopies: HDVE, DPP, and DVE. Each of these intensities is obtained from a sequence of three resonant excitation pulses, separated by time intervals $\tau_1$ and $\tau_2$. The signal is radiated during $\tau_3$. DVE spectroscopy is a homodyne technique that measures the signal field squared. DPP is a self-heterodyned technique whose intrinsic LO is always time coincident with the signal but may be affected by transmission through the sample. The three third-order spectra can be described using signal and LO electric field amplitude and phases as

$$S'_{HDVE}(\tau_1 = 0, \tau_2 = 0, \omega_3;\tau_{LO}) = 2e_{sig}(\omega_3)e_{LO}(\omega_3)\cos[\Delta\phi(\omega_3) + \tau_{LO}\omega_3] \quad (2.10)$$

$$I_{DVE}(\tau_1 = 0, \tau_2 = 0, \omega_3) = e_{sig}(\omega_3)^2 \quad (2.11)$$

$$S'_{DPP}(\tau_1 = 0, \tau_2 = 0, \omega_3;\tau_{LO} = 0) = 2e_{sig}(\omega_3)e_{LO}(\omega_3)\cos[\Delta\phi(\omega_3)] \quad (2.12)$$

where the cross terms have been isolated for HDVE and DPP. As shown in eq 2.3, heterodyne detection produces a cosine term that contains phase and amplitude information. Interfering with an LO provides an amplified signal that scales linearly with $e_{LO}$, $e_{sig}$, and the chromophore concentration. Additionally, DVE and DPP spectra can be extracted from the HDVE spectrum; once the amplitude $e_{LO}e_{sig}$, phase $\Delta\phi(\omega)$, and LO delay $\tau_{LO}\omega$ have been extracted, the DVE spectrum is recreated from $(e_{LO}e_{sig})^2$ and the DPP spectrum is recreated from $e_{sig}e_{LO}\cos(\Delta\phi(\omega))$.

**B. Separation of Amplitude and Phase.** The most challenging part of full signal characterization is the separation of the amplitude and phase components of the measured intensity cross term. We use two distinct methods for extracting these components from the measured HDVE and HFID: Fourier transform spectral interferometry (FTSI)[9,11−14] and phase modulation spectral interferometry (PMSI). Each method extracts the signal field by acquisition of a signal interferogram after introducing a known, frequency-dependent phase shift, $\tau_{LO}\omega$. In FTSI, the spectral interferogram is Fourier transformed back into the time domain, where Kramers−Kronig relations allow for calculation of the imaginary component, $S''$. In PMSI, the local oscillator time delay, and therefore phase, is sinusoidally cycled to extract the imaginary component. Both of these techniques (illustrated in Figure 1) are advantageous because of their simplicity. Each only relies on moving one delay and acquiring the spectral interferogram with an array detector. Other techniques, such as dual-quadrature spectral interferometry and phase cycling, require frequency-independent phase control, which is achieved with waveplates[12] or by pulse shaping,[15] respectively.

***Fourier Transform Spectral Interferometry.*** In FTSI, we use a Kramers−Kronig relationship to relate real and imaginary components of the spectral interferogram. For discussion, we define the double-sided FT, $\tilde{\mathcal{F}}$

$$\tilde{\mathcal{F}}[Z(t)] = \int_{-\infty}^{\infty} dt e^{i\omega t} Z(t) \equiv Z(\omega) \qquad (2.13)$$

and its conjugate single-sided inverse FT, $\tilde{\mathcal{F}}^{-1}$

$$\mathcal{F}^{-1}[Z(\omega)] = \frac{1}{\pi}\int_{0}^{\infty} d\omega e^{-i\omega t} Z(\omega) \equiv Z(t) \qquad (2.14)$$

where $Z$ may be real or complex. The Kramers−Kronig relationship essentially states the equivalence of the single- and double-sided Fourier transforms. Therefore, starting with a real spectral interferogram $S'(\omega;\tau_{LO})$, which is windowed by our detection range to a finite, positive spectrum that spans only the transition of interest, $\mathcal{F}^{-1}[S'(\omega;\tau_{LO})]$ gives a complex time-domain signal $\tilde{S}(t)$ with the property $\tilde{S}(t) = \tilde{S}(-t)^*$. $\tilde{S}(t)$ contains negative and positive time delay components that are symmetrically shifted by $\tau_{LO}$ as a result of $\mathcal{F}^{-1}[Z(\omega)\exp[\pm i\tau_{LO}\omega]] = \tilde{Z}(t \pm \tau_{LO})$. By windowing off one component, the symmetry is broken and the full complex spectrum $\tilde{S}$ is recovered after FT back to the frequency domain

$$\tilde{\mathcal{F}}[W(t)\mathcal{F}^{-1}[S'(\omega;\tau_{LO})]] = \tilde{S}(\omega;\tau_{LO}) = \tilde{E}_{sig}(\omega)\tilde{E}^*_{LO}(\omega)\exp[i\tau_{LO}\omega] \qquad (2.15)$$

$W(t)$ is the windowing function. In our case, this is chosen to be the Heaviside step function, $H(0)$, which removes both DC noise and the negative time signal.

***Phase Modulation Spectral Interferometry.*** The signal amplitude and phase may also be extracted through phase modulation spectral interferometry (PMSI). In this technique, a small time step, $2d\tau$, modulates $\tau_{LO}$ to create a frequency-dependent phase shift that allows for the separation of the real and imaginary parts of the heterodyned intensity based on trigonometric relationships

$$S'(\omega;\tau_{LO}) = \frac{S'(\omega;\tau_{LO} - d\tau) + S'(\omega;\tau_{LO} + d\tau)}{2\cos(d\tau\omega)} \qquad (2.16)$$

$$S''(\omega;\tau_{LO}) = \frac{S'(\omega;\tau_{LO} - d\tau) - S'(\omega;\tau_{LO} + d\tau)}{2\sin(d\tau\omega)} \qquad (2.17)$$

After taking the sum and difference, $\sin(d\tau\omega)$ and $\cos(d\tau\omega)$ are divided out to leave the desired complex HDVE or HFID

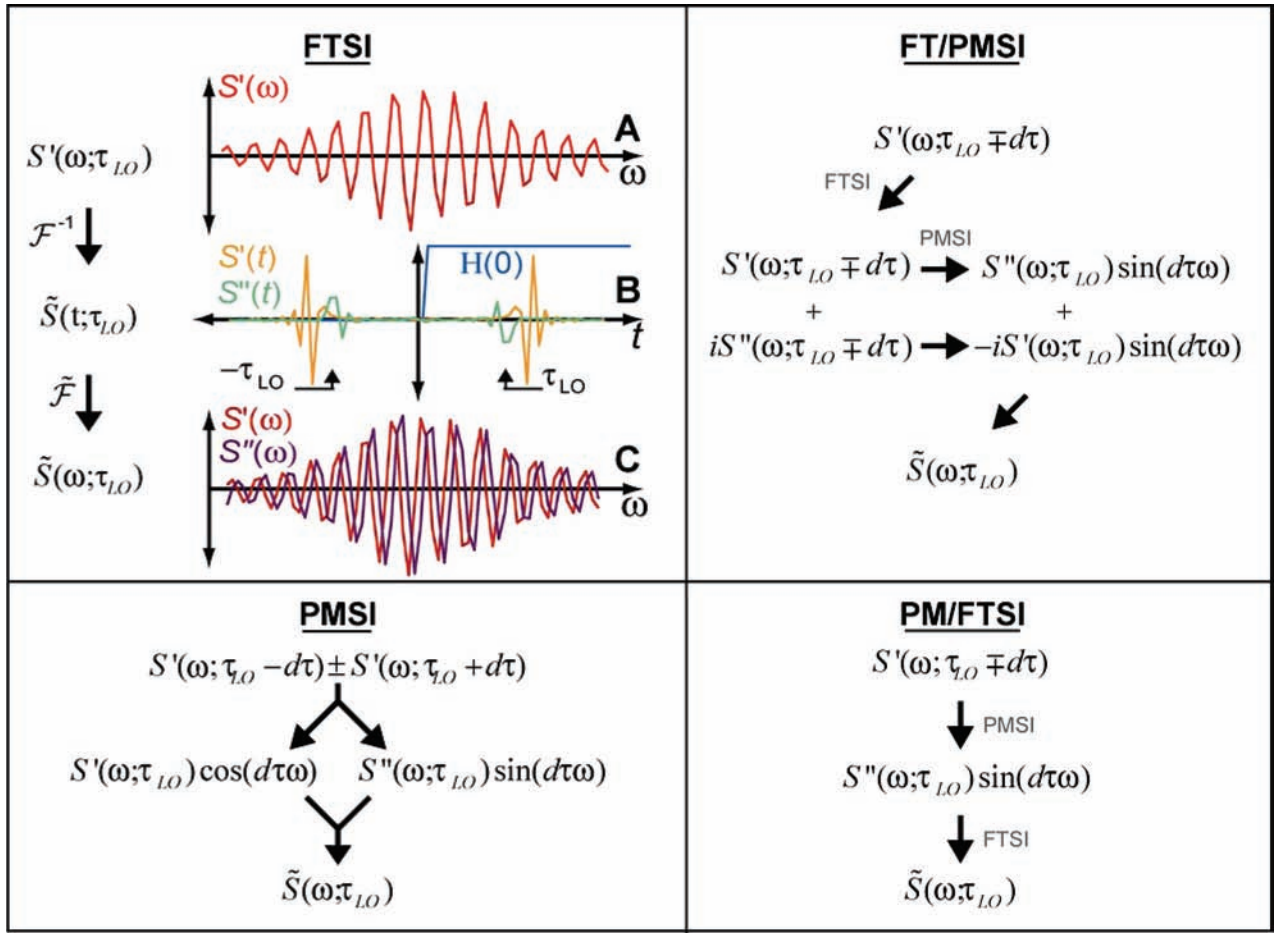


**Figure 1.** Four methods for calculating the complex heterodyned intensity, $\tilde{S}$, from the measured, real projection, $S'$, are described with equations and diagrams. FTSI: The real, asymmetric interferogram (A) is inversely Fourier transformed into the time domain (B) to give a complex time domain signal in which $\mathcal{F}^{-1}[\tilde{E}_{sig}\tilde{E}^*_{LO}e^{i\tau_{LO}\omega}]$ and $\mathcal{F}^{-1}[\tilde{E}^*_{sig}\tilde{E}_{LO}e^{-i\tau_{LO}\omega}]$ components are separated onto the positive and negative time axes. After applying a Heaviside window function to isolate one of these components, Fourier transformation back into the frequency domain gives the complex intensity (C). Actual, 64-pixel *N*-methylacetamide data is shown to the right at each stage of the calculation (A−C). PMSI: The difference and sum of the time-stepped measured interferograms are calculated to give the real and imaginary components multiplied by $\cos(d\tau\omega)$ and $\sin(d\tau\omega)$, respectively. Division by these known sinusoidal functions allows for calculation of $\tilde{S}$. FT/PMSI: FTSI is used to calculate $\tilde{S}(\omega;\tau_{LO} - d\tau)$ and $\tilde{S}(\omega;\tau_{LO} + d\tau)$. Real components are subtracted to give $S''(\omega;\tau_{LO})\sin(d\tau\omega)$. Imaginary components are subtracted to give $S'(\omega;\tau_{LO})\sin(d\tau\omega)$. $\tilde{S}(\omega;\tau_{LO})$ is then calculated. PM/FTSI: PMSI is used to calculate the $S''(\omega;\tau_{LO})\sin(d\tau\omega)$ from the measured $d\tau$ shifted interferograms. After division by $\sin(d\tau\omega)$, FTSI allows for the calculation of $\tilde{S}$.

intensities. Noise between $S'(\omega;\tau_{LO} + d\tau)$ and $S'(\omega;\tau_{LO} - d\tau)$ and inaccuracies in $d\tau$ timing may result in high-frequency oscillations in the extracted amplitude and phase.

## III. Experimental Section

The heterodyne techniques were tested with the acquisition of a series of small protein (ribonuclease A, concanavalin A, ubiquitin, insulin) and peptide (*N*-methylacetamide, diglycine) spectra in the amide I region using a 1 kHz repetition rate, nearly transform-limited IR pulses centered at ~1650 $cm^{-1}$ with fwhm bandwidths of 160 $cm^{-1}$ produced as previously described.[5] Signals were detected with ~2 or 4.7 $cm^{-1}$ resolution on a 2 × 64 element mercury cadmium telluride array (IR-0144, Infrared Systems Development) after diffraction off of a 90 or 40 lines/mm grating mounted in a 190 mm monochromator (Triax 190, Jobin Yvon).

The DVE signals were generated by three time-coincident pulses in a boxcar geometry. Unless noted, HDVE spectra were acquired by heterodyne detecting the DVE signal by overlapping with an external LO. The DPP was collected with two time-coincident pulses in a noncollinear geometry. The DPP signal is intrinsically self-heterodyned without an external LO. The HFID signal was generated by a single pulse transmitted through the sample and overlapped with an external LO. Pulses were delayed using retro-reflectors mounted on translation stages (ANT-50 L, Aerotech) with accuracies of ±0.7 fs. The HFID and HDVE spectra were collected at $\tau_{LO} = -4.000$ ps, which provides FTSI time-domain separation for our detection resolution, and at PMSI $d\tau = 2$ fs, which introduces $\sim\pi/2$ phase shift. The DVE spectrum is background free, but scatter was removed by subtracting the background generated by chopping consecutive shots of an excitation beam. The $\tau_{LO} = 0$ was initially set at the time where the HDVE matched the independently measured 2-beam DPP.

The spectral interferogram, $S'$ (eq 2.3), was isolated from the measured intensity, $I$, eq 2.2, after subtracting the squared terms. For HFID, HDVE, and DPP, the $e_{LO}^2$ homodyne term in eq 2.2 was measured by chopping an excitation beam to remove the signal in consecutive shots. For HDVE and DPP, the $e_{sig}^2$ term was ignored because $e_{sig}^2 \ll S'$. For HFID, $e_{sig}^2$ was subtracted through balanced detection.[8,16] For the single-shot HDVE measurements, the $e_{LO}^2$ and $e_{sig}^2$ terms were subtracted through balanced detection using a reference spectrum measured in advance.

The in-phase and in-quadrature components of the heterodyned intensity were used to extract the phase and amplitude. The amplitude was calculated from the modulus squared of the complex spectrum. The phase was calculated using

$$\Delta\varphi(\omega) + \tau_{LO}\omega = \text{atan}(S''(\omega)/S'(\omega)) \qquad (3.1)$$

Due to the cosine nature of the measured heterodyned intensity, only |mod(phase,2$\pi$)| is measured and an unwrapping procedure was applied to obtain the relative offset. The $\tau_{LO}$ was corrected in data processing by up to 4 periods (80 fs) to maximize agreement between the 2-beam DPP and the DPP extracted from the HDVE. Relative times were determined within 0.7 fs (200 nm, $\lambda$/30) from the stage encoder. Slight differences between the directly collected DVE and DPP and their HDVE-extracted counterparts can be attributed to phase and amplitude differences between the external LO and the self-heterodyning beam, which passes through the sample. The LO shaping effects can be corrected through characterization of the HFID phase,[14] but we do not because the unchirped external LO allows for a more faithful measurement of the signal phase.

## IV. Results and Discussion

To validate the FTSI and PMSI methods, we measured complex HDVE and HFID spectra and compared the extracted results with experimental DVE, DPP, IR, and FTIR spectra. The results are shown in Figure 2. Agreement between the conventionally collected and heterodyne-extracted spectra indicated that the DVE and linear IR spectra were readily obtained and faithfully reproduced from the HDVE and HFID spectra, respectively. The DPP may also be recreated with knowledge of $\tau_{LO}$. Although determination of $\tau_{LO}$ was based on matching the HDVE spectral interferogram to the 2-beam DPP, other promising techniques, such as interferometric autocorrelation between the LO and a pinhole-scattered beam at the sample position,[17,18] may be used to determine $\tau_{LO}$ with <1 fs accuracy without the 2-beam DPP spectrum. Slight inconsistencies between the spectra are attributed to slight phase and amplitude differences between the internal and the external LO.

For FTSI, the upper and lower bounds of the $|\tau_{LO}|$ timing are limited by the ability to properly separate and sample both wings of the Fourier-transformed interferogram. Large values of $|\tau_{LO}|$ induce rapid spectral oscillations that cannot be sampled. Thus, the upper bound is dictated by the Nyquist period, $(2\Delta\omega c)^{-1}$, where $\Delta\omega$ is the frequency difference between consecutive pixels and $c$ is the speed of light. The lower bound on $|\tau_{LO}|$ is set by the pulse widths and the range of sampled frequencies; at small, negative LO timings, the positive and negative time components of $\tilde{S}(t;\tau_{LO})$ mix, preventing correct recovery of the complex frequency spectra. At $\tau_{LO} = 0$, finite pulse effects and DC contributions can also lead to mixing of the conjugate signals and distortions that affect the recovered frequency spectra. Therefore, a $\tau_{LO}$ of at least a few pulse widths is ideal.

For PMSI, the maximum $|\tau_{LO}|$ is limited to the Nyquist period by undersampling but there are no restrictions on the minimum. The time step, $2d\tau$, should be chosen so that the center frequency is shifted by $\sim\pi/2 + n\pi$, where $n$ is an integer, and the phase shifts across the spectrum are within $\pm\pi/4$ of the central frequency shift to avoid zero crossings in $\sin(d\tau\omega)$ and $\cos(d\tau\omega)$. Oscillations in our extracted PMSI spectra indicate noise and errors in timing. To correct for inaccuracies in measured time delays, the HFID timings $d\tau$ were adjusted in data processing by up to 0.5 fs to remove oscillations from the PMSI-extracted absorbance and phase spectra.

**Extension to Combination Methods.** Combinations of the FTSI and PMSI methods described above can be used to eliminate noise and subtract away homodyne components. This, in some cases, precludes the need for a chopping scheme. FT/PMSI and PM/FTSI use FTSI followed by PMSI, or vice versa, to calculate the complex spectrum from $S'(\omega;\tau_{LO} + d\tau)$ and $S'(\omega;\tau_{LO} - d\tau)$. Both methods are shown schematically in Figure 1. The combination methods are advantageous because they rely on subtraction, which allows for removal of noise and homodyne components. When combined with balanced detection, which measures the 0 and $\pi$ phase components of the signal, the FT/PMSI calculates and appropriately subtracts the $\pi/2$ and $3\pi/2$ components in a method analogous to NMR quadrature detection with a similar resulting reduction in noise. Through subtraction, the PM/FTSI method removes the $e_{LO}^2$ and $e_{sig}^2$ terms from the measured intensity, which allows for the extraction of the amplitude and phase without chopping and without balanced detection. The FT/PMSI and PM/FTSI methods are used to extract the DPP, DVE, and IR spectra of concanavalin A as shown in Figure 2.

As our results show, the FTSI reproduces the spectra with the greatest fidelity. FTSI can be done with a single laser shot,

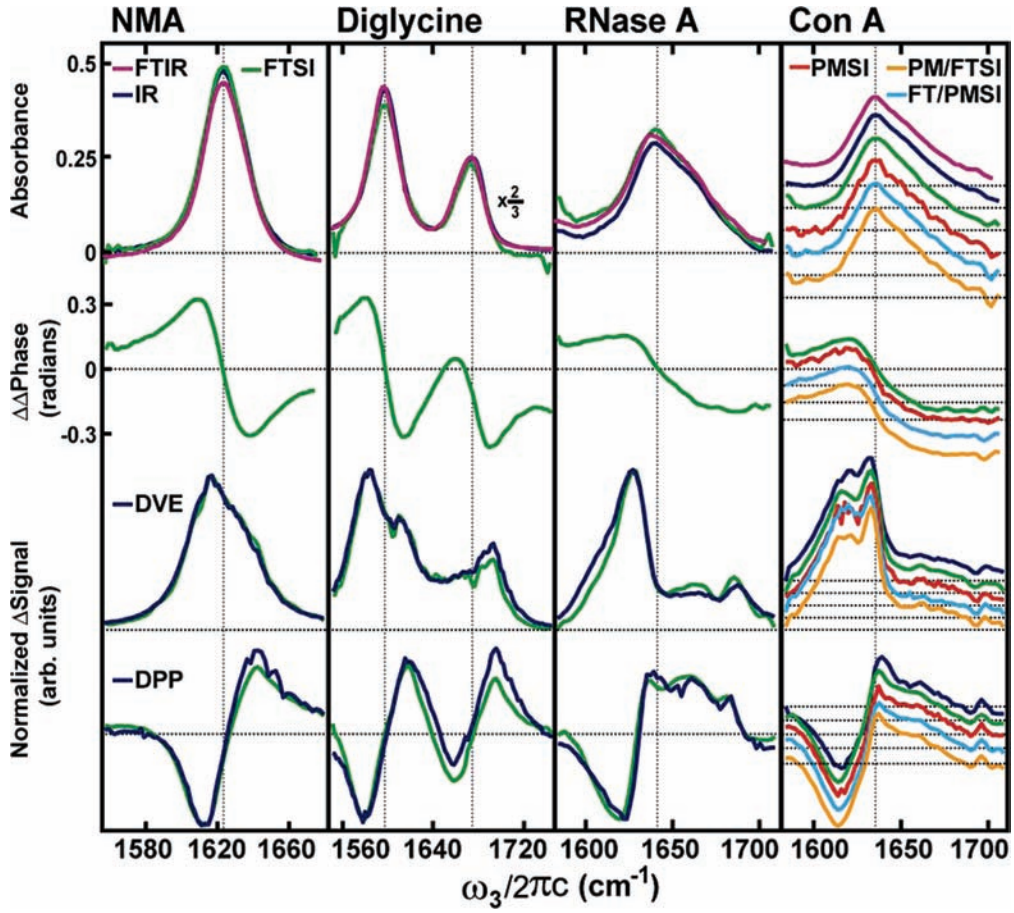


**Figure 2.** Linear absorbance, linear phase, DVE, and DPP spectra (rows, respectively) are plotted for *N*-methylacetamide, diglycine, ribonuclease A, and concanavalin A samples (columns, respectively). FTIR (purple, row 1), IR (blue, row 1), DVE (blue, row 3), and DPP (blue, row 4) spectra are compared to their FTSI (green), PMSI (red, column 4), FT/PMSI (teal, column 4), and PM/FTSI (orange, column 4) heterodyne-extracted counterparts. For the ΔΔphase plots (row 2), the absolute zero is chosen arbitrarily. The HDVE, DVE, and DPP spectra were each averaged for 5 min. The HFID protein and solvent measurements were each averaged for 15−20 min.

but applying eq 2.15 to truncated spectra adds noise and ripples. PMSI does not rely on Kramers−Kronig relations, and truncation does not affect the characterization, but inaccuracies in timing and noise between time-stepped spectra lead to ripples in the recovered phase and amplitude. Improvements in the accuracy of time stepping beyond the $\lambda/30c$ resolution here, in addition to shot-to-shot $\tau_{LO}$ modulation, can be implemented with piezoelectric actuators. Given ideal collection schemes with improved $\tau_{LO}$ stepping and frequency detection that spans the transition of interest, the FT/PMSI- and PM/FTSI-extracted spectra should best match the conventional spectra and have the least noise.

A further characterization of the detection linearity is shown in Figure 3. The linear concentration dependence of the HDVE amplitude and square concentration dependence of the DVE amplitude are verified by plotting the measured DVE intensity and FTSI-extracted $e_{sig}e_{LO}$ intensity at varying concentrations of NMA, as shown as a log−log plot in Figure 3a. The linear fits indicate the expected linear and squared dependencies for the HDVE and DVE intensities. For our laser stability and 15 bit detection depth, heterodyne detection of the DVE increases the measured intensity by a factor of 5, which not only allows for simultaneous extraction of DPP and DVE spectra of micromolar protein samples but also indicates that equivalent signal-to-noise measurements can be made in less than twice the time of current DVE and DPP collection techniques.

As an example of an HDVE application, Figure 3b shows a comparison of the melting curve for thermal unfolding of ubiquitin extracted using singular value decomposition analysis on a set of DVE and HDVE spectra acquired at temperatures spanning the unfolding temperature. This measurement is desirable for obtaining a measure of the folded population at different temperatures. The importance of the linear detection is illustrated by the sharper transition observed by HDVE. This can be rationalized considering that the DVE is proportional to the amplitude squared, while the HDVE is linearly proportional to the amplitude.

The sensitivity of HDVE for protein applications is illustrated through a characterization of the equilibrium constant for the monomer-to-dimer transition of insulin (Figure 4). Formation of the dimer of the largely helical protein leads to the folding of an intermolecular $\beta$ sheet at the dimer interface, allowing monomer and dimer to be distinguished from the relative intensities of α-helical and $\beta$-sheet regions of the amide I spectrum. Concentration-dependent HDVE amplitude spectra are shown for predominately dimeric, high (7.0 mM) and predominately monomeric, low (180 $\mu$M) insulin concentrations. The ratio of HDVE amplitudes integrated across the α-helical region of the monomer (1642−1652 cm$^{-1}$) and the $\beta$-sheet region of the dimer (1614−1633 cm$^{-1}$)[6] are fit to the Hill equation: $\theta(c) = (c^n)/(K_D^n + c^n)$, where $K_D$ is the dissociation constant, $c$ is the insulin concentration, and $n$ is the Hill coefficient.[19] This fit leads to a value of $K_D = 3.3$ mM for $T =$ 22 °C and for a sample with 10% EtOD and 0.27 M DCl. For an ideal measurement of the dissociation constant, the chosen concentrations should span orders of magnitude across $K_D$. The

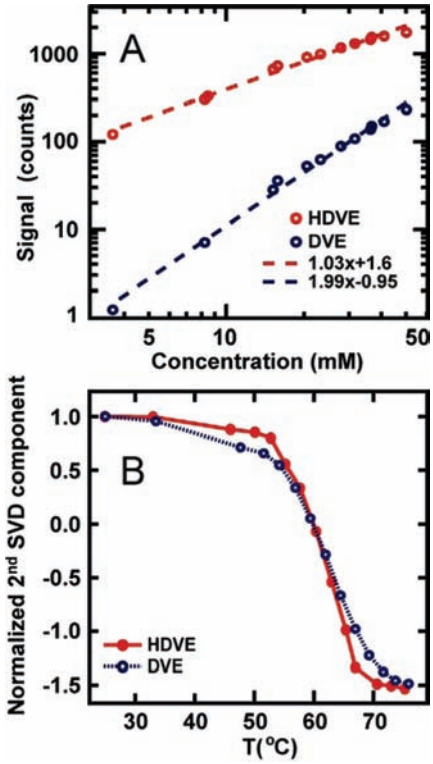


**Figure 3.** (A) *N*-Methylacetamide 1619 $cm^{-1}$ HDVE (red) and DVE (blue) peak intensities are plotted versus concentration. The log/log plot lines of best fit have slopes of 1.03 ± 0.03 (HDVE) and 1.99 ± 0.05 (DVE). Each point is the result of 5 min of averaging. (B) Normalized second SVD components derived from temperature-dependent HDVE (red) and DVE (blue) spectra of ubiquitin are plotted versus temperature. Each point is the result of 10 min of averaging.

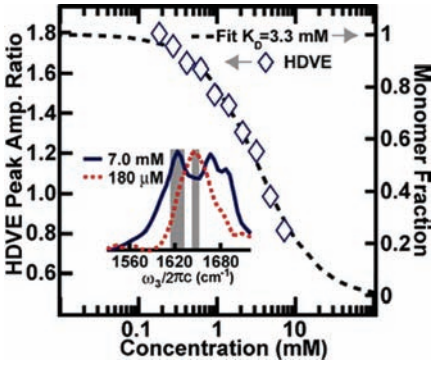


**Figure 4.** (Left axis) Insulin FTSI HDVE amplitude peak ratios are plotted versus concentration. (Inlay) Lowest (180 $\mu$M, dotted red line) and highest (7.0 mM, solid blue line) concentration spectra are plotted. The gray bars indicate the integrated spectral regions used for the peak ratios. The 1642−1652 $cm^{-1}$ integrated area is divided by the 1614−1633 $cm^{-1}$ area. (Right axis) Ratios are fit to the Hill equation to extract a $K_D$ = 3.3 mM and an $n$ = 1.1. Insulin was dissolved in 10% EtOD and 0.27 M DCl. Each spectrum was collected on the less dispersive grating for 2 min at $\tau_{LO}$ = 1.500 ps with an internal LO passing through the sample ~30 ps after the other IR beams.

amplification characteristics of HDVE allow for these necessary low concentration measurements, which are not accessible with current DVE intensities.

HDVE may also be used as a single-shot technique to extract the DVE and DPP spectra from a single measurement. HDVE is advantageous because it can be collected without scanning time delays and allows for the separation of phase and amplitude. Figure 5 compares the ubiquitin DVE and DPP spectra and their corresponding single-shot HDVE-extracted counterparts. Five hundred shots are averaged and shown with standard deviations. Agreement between the single-shot HDVE and DVE and DPP spectra suggests that HDVE measurements may be used in low repetition or irreversible measurements where only unusually high absorption changes could be measured with conventional 2-beam pump−probe acquisition.

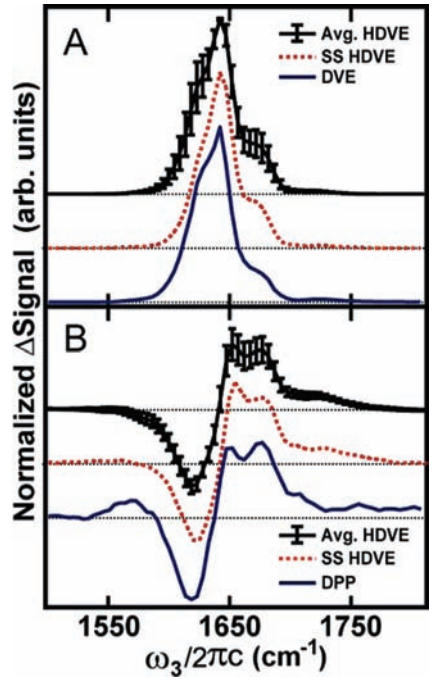


**Figure 5.** Fifteen milligram per milliliter ubiquitin: (A) DVE (blue, solid line), single-shot HDVE-extracted amplitude squared (red, dotted line), 500-shot averaged HDVE-extracted amplitude squared (black, solid line) and (B) DPP (blue, solid line), single-shot HDVE-extracted DPP (red, dotted line), 500-shot averaged HDVE-extracted DPP (black, solid line) spectra are plotted. The standard deviation of the averaged HDVE-extracted spectra are shown. Spectra were collected at a 200 fs waiting time on the less dispersive grating at $\tau_{LO}$ = 1.000 ps with an internal LO. The DVE and DPP spectra were collected for 2.5 min.

## V. Conclusion

Heterodyne detection is a powerful technique that amplifies signals, allows for measurement of the amplitude and phase, and generates a measurement that is linear to the electric field of the signal, which is in turn linear in concentration. The trade off is additional complexity in alignment and an ambiguity in the absolute timing between LO and signal. We demonstrated that HDVE is a one-dimensional complement to 2D IR, which can be applied in single-shot mode. Through FTSI, PMSI, or a combination of the two, both the linear and the third-order signal can be completely characterized as an amplitude and a phase, which allows for simultaneous extraction of the DVE and DPP or IR absorbance spectra. PMSI was also introduced as a complementary phase and amplitude determination technique that does not rely on pulse shapers or FT calculations. HDVE will be particularly valuable in experiments that have previously relied on DVE and DPP measurements, such as low concentration protein studies and low repetition rate temperature jump experiments, in which signal-to-noise ratios are small.

**Acknowledgment.** This work was supported by the National Science Foundation (CHE-0616575 and CHE-0911107).

## References and Notes

(1) Ganim, Z.; Chung, H. S.; Smith, A. W.; DeFlores, L. P.; Jones, K. C.; Tokmakoff, A. *Acc. Chem. Res.* **2008**, *41*, 432.

(2) Chung, H. S.; Khalil, M.; Smith, A. W.; Ganim, Z.; Tokmakoff, A. *Proc. Natl. Acad. Sci. U.S.A.* **2005**, *102*, 612.

(3) Hamm, P.; Lim, M.; DeGrado, W. F.; Hochstrasser, R. M. *J. Chem. Phys.* **2000**, *112*, 1907.

(4) Krummel, A. T.; Zanni, M. T. *J. Phys. Chem. B* **2006**, *110*, 13991.

(5) Khalil, M.; Demirdoven, N.; Tokmakoff, A. *J. Phys. Chem. A* **2003**, *107*, 5258.

(6) Chung, H. S.; Khalil, M.; Tokmakoff, A. *J. Phys. Chem. B* **2004**, *108*, 15332.

(7) de Boeij, W. P.; Pshenichnikov, M. S.; Wiersma, D. A. *Chem. Phys.* **1998**, *233*, 287.

(8) Asplund, M. C.; Zanni, M. T.; Hochstrasser, R. M. *Proc. Natl. Acad. Sci. U.S.A.* **2000**, *97*, 8219.

(9) Ferro Albrecht, A.; Hybyl, J. D.; Jonas, D. M. *J. Chem. Phys.* **2001**, *114*, 4649.

(10) Kindt, J. T.; Schmuttenmaer, C. A. *J. Phys. Chem.* **1996**, *100*, 10373.

(11) Kuajwinska, M. Spatial Phase Measurement Methods. In *Interferogram Analysis: Digital Fringe Pattern Measurement Techniques*; Institute of Physics Publishing: Bristol, U.K., 1993.

(12) Lepetit, L.; Cheriaux, G.; Joffre, M. *J. Opt. Soc. Am. B* **1995**, *12*, 2467.

(13) Dorrer, C.; Belabas, N.; Likforman, J.-P.; Joffre, M. *J. Opt. Soc. Am. B* **2000**, *17*, 1795.

(14) Gallagher, S. M.; Albrecht, A. W.; Hybl, J. D.; Landin, B. L.; Rajaram, B.; Jonas, D. M. *J. Opt. Soc. Am. B* **1998**, *15*, 2338.

(15) Shim, S.-H.; Strasfeld, D. B.; Ling, Y. L.; Zanni, M. T. *Proc. Natl. Acad. Sci. U.S.A.* **2007**, *104*, 14197.

(16) In balanced detection, after the signal and LO are combined on a beam splitter, both transmitted and reflected interferograms are collected and subtracted to remove homodyne components. A 180° phase shift is introduced between the reflected and the transmitted interferograms due to the presence of an internal reflection in one arm of the setup.

(17) Bristow, A. D.; Karaiskaj, D.; Dai, X.; Cundiff, S. T. *Opt. Express* **2008**, *16*, 18017.

(18) Backus, E. H. G.; Garrett-Roe, S.; Hamm, P. *Opt. Lett.* **2008**, *33*, 2665.

(19) Barcroft, J.; Hill, A. V. *J. Physiol.* **1910**, *39*, 411.

JP906256S